

A spatial analog of the Ruelle-Takens-Newhouse scenario developing in reactive miscible fluids

Dmitri Bratsun

Department of Applied Physics,
Perm National Research Polytechnical University,
Perm, 614990, Russia
E-mail: dmitribratsun@rambler.ru

June 6, 2019

Abstract

We present a theoretical study on pattern formation occurring in miscible fluids reacting by a second-order reaction $A + B \rightarrow S$ in a vertical Hele-Shaw cell under constant gravity. We have recently reported that concentration-dependent diffusion of species coupled with a frontal neutralization reaction can produce a multi-layer system where low density depleted zones could be embedded between the denser layers. This leads to the excitation of chemoconvective modes spatially separated from each other by a motionless fluid. In this paper, we show that the layers can interact via a diffusion mechanism. Since diffusively-coupled instabilities initially have different wavelengths, this causes a long-wave modulation of one pattern by another. We have developed a mathematical model which includes a system of reaction-diffusion-convection equations. The linear stability of a transient base state is studied by calculating the growth rate of the Lyapunov exponent for each unstable layer. Numerical simulations supported by the phase portrait reconstruction and Fourier spectra calculation have revealed that nonlinear dynamics consistently passes through (i) a perfect spatially periodic system of chemoconvec-

tive cells; (ii) a quasi-periodic system of the same cells; (iii) a disordered fingering structure. We show that in this system, the coordinate co-directed to the reaction front paradoxically plays the role of time, time itself acts as a bifurcation parameter, and a complete spatial analog of the Ruelle-Takens-Newhouse scenario of the chaos onset is observed.

In recent decades, the study of the interaction between reaction-diffusion phenomena and convective instabilities brought many surprises. Let us focus on a neutralization reaction: a second-order $A + B \rightarrow C$ reaction is distinguished by a comparatively simple, albeit nonlinear, kinetics. If two species are initially separated in space, the reaction proceeds in a frontal manner due to the high value of the reaction rate constant. In this case, it may result in various buoyancy-driven instabilities if the reaction occurs either in immiscible two-layer systems [1, 2, 3, 4, 5] or in miscible acid-base systems [6, 7, 8, 9, 10, 11, 12, 13, 14, 15, 16]. Among the important effects that have been observed here, we highlight the pattern convection in the form of a perfectly periodic system of cellular-like fingers keeping contact with the interface when an organic solvent containing an acid A is in contact with an aqueous solution of an inorganic base B [3]. At that time, a liquid-liquid interface has been recognized as the main reason for this unusual regularity of salt fingering [2, 5]. However, then a perfectly organized structure of fingers has been observed already in the miscible system, where two aqueous solutions of base and acid have been brought into contact [13, 15]. It was shown that this pattern arises due to the strong dependence of the diffusion coefficients of the initial reactants and the reaction product on their concentrations. The effect of concentration-dependent diffusion (hereinafter CDD) coupled with a fast neutralization reaction has been demonstrated to produce a spatially localized zone with unstable density stratification (figuratively, a density pocket) in a system with inherently stable configuration, when a less dense solution is placed above a more dense one. It should be noted that such an effect creates a new situation in fluid mechanics when the convective modes arise in different parts of the medium and compete on the distance. In this case, the patterns can be coupled by the diffusion of heat or matter which transmit a signal through an interlayer of the motionless fluid.

Generally, the CDD effect means a significant expansion of the degrees of freedom for the system to produce various types of instabilities and nonlinear dynamics that do not fit into the traditional classification [14]. For example,

we have shown recently that when varying initial concentrations of solutions, the density pocket may collapse suddenly, causing a density shock wave separating the fluid at rest and the area with anomalously intense convective mixing [16].

In this communication, we study the nonlinear interaction between two periodic systems of chemoconvective cells that arise independently inside two different layers low in density. Although initially the layers are separated by the motionless fluid, they can nevertheless influence each other via the diffusion of the reactants. Thus, this configuration reproduces the conditions for the realization of a spatial analog of the Ruelle-Takens-Newhouse scenario of the transition to chaos. As it is known, the Ruelle-Takens-Newhouse theory [17, 18] postulates that the power spectrum of a dynamical system evolves as a function of the control parameter and at the beginning consists of one frequency, then two (sometimes three), and then the broadband noise characteristic of chaos should start to appear. In our case, we demonstrate that a similar sequence of bifurcations is reproduced, but the role of time is played by the spatial horizontal coordinate with time itself now being a control parameter.

Mathematical model. – We consider two aqueous solutions of acid A and base B filling the cavity, which is strongly compressed in one of directions, so that the Hele-Shaw (HS) approximation is applied. Right after the process starts, the reagents with initial concentrations A_0, B_0 diffuse into each other and are neutralized at the rate k with the formation of salt C . Since both reagents are dissolved in water, their mixing begins at the contact of initially separated layers. It is noteworthy that the problem is non-autonomous because reagents are not replenished during the reaction and concentration profiles change irreversibly. Generally, a neutralization reaction is known to be exothermic. However, in this paper, the heat release is neglected. In experiments, one can always achieve such reaction conditions, if the walls of the HS cell are made quite conductive for heat to dissipate. In what follows, we assume that $A_0 = B_0$.

The system geometry is given by a two-dimension domain defined by $0 \leq x \leq L$, $-H \leq z \leq H$ with x -axis directed horizontally and z -axis anti-directed to gravity. We scale the problem by using $2d$, $4d^2/D_{a0}$, $D_{a0}/2d$, A_0 as the length, time, velocity and concentration scales, respectively. D_{a0} , ν , c_p , d stands for acid diffusivity (table value), kinematic viscosity and the HS semi-gapwidth.

The mathematical model we develop consists in the set of equations for

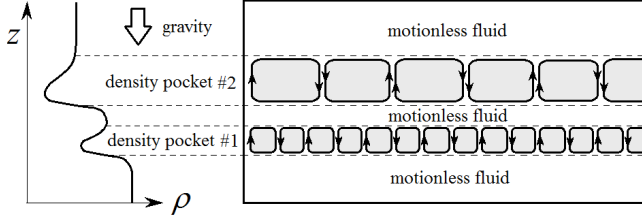


Figure 1: Schematic presentation of two systems of convective rolls independently arising in a depleted zone low in density.

species coupled to Navier-Stokes equation written in the HS approximation [13]:

$$\Phi + \nabla^2 \Psi = 0, \quad (1)$$

$$\frac{1}{Sc} \left(\partial_t \Phi + \frac{6}{5} J(\Psi, \Phi) \right) = \nabla^2 \Phi - 12\Phi - \partial_x \rho, \quad (2)$$

$$\partial_t A + J(\Psi, A) = \nabla(D_a(A)\nabla A) - \alpha AB, \quad (3)$$

$$\partial_t B + J(\Psi, B) = \nabla(D_b(B)\nabla B) - \alpha AB, \quad (4)$$

$$\partial_t C + J(\Psi, C) = \nabla(D_c(C)\nabla C) + \alpha AB, \quad (5)$$

$$\rho = R_a A + R_b B + R_c C, \quad (6)$$

where $J(F, P) \equiv \partial_z F \partial_x P - \partial_x F \partial_z P$ stands for the Jacobian determinant. Here we use a two-field formulation for the motion equation, and introduce the stream function Ψ and vorticity Φ . The diffusion terms in Eqs. (3-5) are written in the most general form, allowing the concentration-dependent phenomena [19]. The problem involves following dimensionless parameters:

$$Sc = \frac{\nu}{D_{a0}}, \quad \alpha = \frac{4kA_0 d^2}{D_{a0}}, \quad R_i = \frac{8g\beta_i A_0 d^3}{\nu D_{a0}}, \quad (7)$$

which are the Schmidt number, the Damköhler number, and the set of solutal Rayleigh numbers, where $i = \{a, b, c\}$, respectively. Eqs. (1-6) should be supplemented by the boundary conditions

$$\begin{aligned} x = 0, L : \Psi = \partial_x \Psi = 0, \quad \partial_x A = 0, \quad \partial_x B = 0, \quad \partial_x C = 0 \\ z = \pm H : \Psi = \partial_z \Psi = 0, \quad \partial_z A = 0, \quad \partial_z B = 0, \quad \partial_z C = 0 \end{aligned} \quad (8)$$

and the initial conditions at $t = 0$:

$$\begin{aligned} z \leq 0 : \quad \Psi = 0, \quad A = 0, \quad B = 1; \\ z > 0 : \quad \Psi = 0, \quad A = 1, \quad B = 0. \end{aligned} \quad (9)$$

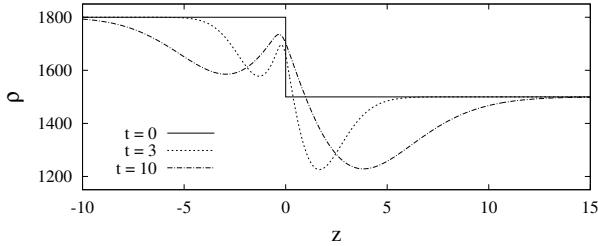


Figure 2: Instantaneous base state profiles of the density ρ are plotted against the vertical axis z at times $t = 0, 3, 10$.

We have shown in [13, 15] that the coupling between a second order reaction and nonlinear diffusion can transform an initially stably stratified fluid layer to a multi-layered system where the depleted zones low in density are embedded between the denser layers. This situation is presented schematically in Fig. 1. The figure shows a vertical density profile with two local minima, which can be defined as low-density pockets. It is important to note that the fluid layer shown in Fig. 1 remains globally stable, since locally unstable fluid sublayers are not able to set in motion the adjacent immobile fluid. By changing the type of chemical reaction, the involved reagents, or their initial concentrations, we can create quite diverse configurations of the vertical stratification of the system. In order to proceed further, it is necessary to specify closed-form exact laws of diffusion in (3-5). The problem is that so far the CDD effect has been underestimated in fluid mechanics. Therefore, data on the concentration-dependence of the diffusion coefficients has appeared to be fragmentary and incomplete for most substances. In what follows we use the diffusion laws developed recently for the pair HNO_3/NaOH (for more details, see [13]):

$$\begin{aligned}
 D_a(A) &\approx 0.881 + 0.158A, \\
 D_b(B) &\approx 0.594 - 0.087B, \\
 D_c(C) &\approx 0.478 - 0.284C.
 \end{aligned}
 \tag{10}$$

The values of the parameters (7) for the pair HNO_3/NaOH can be estimated as follows: $Sc = 317$, $\alpha = 10^3$, $R_a = 3.2 \times 10^5$, $R_b = 3.8 \times 10^5$, $R_c = 5.1 \times 10^5$.

Dynamics of the base state and its stability. – The system of equations (1-10) allows the base state that describes the dynamics of pure reaction-diffusion processes. In this state, the fluid is at rest all the time. We assume

that the fluid velocity is zero and concentration fields depends only on the vertical coordinate z and time t : $A_0(t, z)$, $B_0(t, z)$, $C_0(t, z)$. Then we obtain:

$$\begin{aligned}\partial_t A_0 &= D_a(A_0)\partial_{zz}A_0 + \partial_z D_a(A_0)\partial_z A_0 - \alpha A_0 B_0, \\ \partial_t B_0 &= D_b(B_0)\partial_{zz}B_0 + \partial_z D_b(B_0)\partial_z B_0 - \alpha A_0 B_0, \\ \partial_t C_0 &= D_c(C_0)\partial_{zz}C_0 + \partial_z D_c(C_0)\partial_z C_0 + \alpha A_0 B_0.\end{aligned}\tag{11}$$

The problem (8-11) can be solved only numerically.

Fig. 2 shows the base state profiles of the density $\rho(t, z)$ defined by (6) for three consecutive times $t = 0, 3, 10$. The system starts to evolve from the initial state, in which the lighter acid solution ($z \geq 0$) is above the more dense base solution ($z < 0$). Thus, there exists a stable vertical stratification in terms of density, which excludes the development of Rayleigh-Taylor instability. As soon as reaction-diffusion processes begin, the density profile undergoes dramatic changes: now it has two minima located above and below the reaction front implying a possible development of local instabilities in the depleted zones low in density. Thus, the formal scheme shown in Fig. 1 is reproduced in practice. The mechanism of the formation of such a multi-layered system has been discussed in detail in [13, 15]. Here we just briefly note that the main reason is that the reaction product starts to be deposited near the reaction front. Since the diffusion coefficient of salt decreases with the growth of its concentration (the CDD effect), it can progressively accumulate near the reaction front making a local maximum in the density profile (Fig. 2, $t = 3$). Since the acid has a higher value of the diffusion coefficient, over time, this maximum slowly shifts down (Fig. 2, $t = 10$). Thus, the diffusion makes the system to be non-autonomous, and time is the control parameter of the system.

Let us analyze the stability of a time-dependent base state defined by Eqs. (10,11) with respect to small monotonic perturbations:

$$\begin{pmatrix} \Phi(t, x, z) \\ \Psi(t, x, z) \\ A(t, x, z) \\ B(t, x, z) \\ S(t, x, z) \end{pmatrix} = \begin{pmatrix} 0 \\ 0 \\ A_0(t, z) \\ B_0(t, z) \\ S_0(t, z) \end{pmatrix} + \begin{pmatrix} \varphi(t, z) \\ \psi(t, z) \\ a(t, z) \\ b(t, z) \\ c(t, z) \end{pmatrix} e^{Ikx}, \tag{12}$$

where φ, ψ, a, b, c are, respectively, the amplitudes of normal form perturbations for the vorticity, stream function, acid, base and salt concentrations

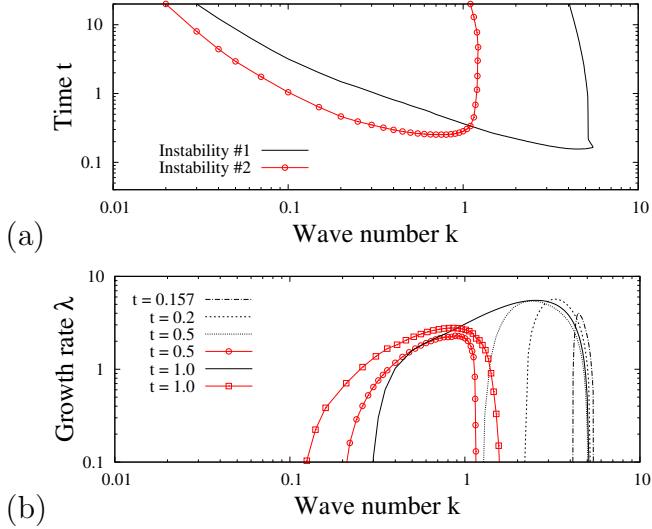


Figure 3: (color online). (a) Neutral curves for two instabilities which arise in two zones low in density shown in Fig. 2; (b) Real part of the growth rate of the instability #1 (lines) and #2 (line-points) are illustrated at different times.

while k is their wavenumber. Substituting (12) into Eqs. (1-6) and linearizing these equations near the base state (11), we obtain the following system of time-dependent amplitude equations for the determination of critical perturbations:

$$\begin{aligned}
\phi + \partial_{zz}\psi - k^2\psi &= 0, \\
\frac{1}{Sc}\partial_t\phi &= \partial_{zz}\phi - (k^2 + 12)\phi - k^2(R_a a + R_b b + R_c c), \\
\partial_t a &= D_a(A_0)(\partial_{zz}a - k^2a) + D'_a(2\partial_z A_0\partial_z a + a\partial_{zz}A_0) \\
&\quad - \alpha(A_0 b + aB_0) - \psi\partial_z A_0, \\
\partial_t b &= D_b(B_0)(\partial_{zz}b - k^2b) + D'_b(2\partial_z B_0\partial_z b + b\partial_{zz}B_0) \\
&\quad - \alpha(A_0 b + aB_0) - \psi\partial_z B_0, \\
\partial_t c &= D_c(C_0)(\partial_{zz}c - k^2c) + D'_c(2\partial_z C_0\partial_z c + c\partial_{zz}C_0) \\
&\quad + \alpha(A_0 b + aB_0) - \psi\partial_z C_0,
\end{aligned} \tag{13}$$

where the linearization is carried out taking into account the explicit form of the diffusion laws (10).

In order to determine the stability of a time-dependent base state, we apply the method of the initial value problem (IVP). As it was shown in [20], the IVP calculation gives essentially the same results as the quasi-steady-state approach, except for a short period of time in which the base state changes rapidly. In our case, the system becomes unstable only after some critical period of time and the IVP usage is reasonable [2]. Thus, Eqs. (13) are numerically integrated together with the base state problem (8-11) and the boundary conditions for disturbances

$$z = \pm H : \quad \phi = 0, \quad \partial_z a = 0, \quad \partial_z b = 0, \quad \partial_z c = 0 \quad (14)$$

to compute the growth rate λ defined similarly to the Lyapunov exponent:

$$\lambda(t) = \frac{1}{N} \sum_{j=1}^N \frac{1}{\Delta t} \ln \frac{a_j(t + \Delta t, z_{min})}{a_j(t, z_{min})}, \quad (15)$$

where Δt is the integration time step and N is the number of independent realizations (typically 10-15). Because the growth rate λ is sensitive to the given initial data, each independent integration started from white noise with an amplitude less than 10^{-4} . We have fixed the occurrence of instability to the time when $\lambda(t)$ averaged over N realizations changes sign from negative to positive. The position z_{min} for measuring λ was chosen at one of the local minima shown in Fig. 2.

Fig. 3a presents neutral curves for two instabilities which arise independently. The instability #1 below the reaction front (in fact, the CDD instability) develops first. The minimum of the neutral curve corresponds to the wave number $k_1 \approx 4.4$ at time $t_1 \approx 0.156$. The instability #2 starts at $k_2 \approx 0.75$ and $t_2 \approx 0.253$. Fig. 3b presents the instantaneous growth rates λ as a function of k calculated for both instabilities. Although the sublayers are separated by the immobile fluid, the instabilities still can influence each other through a diffusion mechanism (Fig. 3b, $t = 0.5, 1.0$). One can see that at times $t > 0.5$, the lower instability #1 can no longer develop independently: its range of unstable waves expands dramatically due to longer waves, which can be explained by the influence of the instability #2 developing in the same range of long waves. Fig. 3 demonstrates also that the wavelength ratio of the fastest growing disturbances varies with time, both due to the diffusive expansion of the density pockets and their mutual influence.

Nonlinear dynamics. – We now discuss the results of direct numerical simulation of the problem (1-10). To see a non-linear development of the

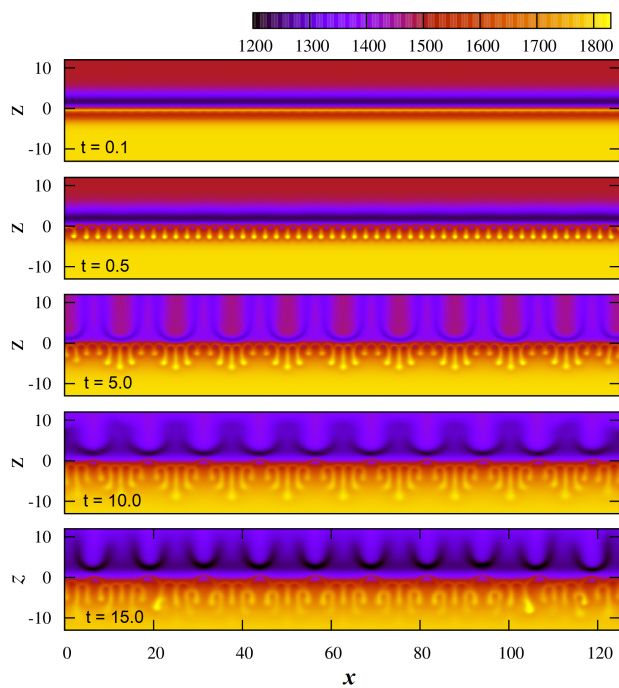


Figure 4: (color online). Nonlinear evolution of the total density ρ with time. The frames from up to down pertain to times $t = 0.1, 0.5, 5, 10, 15$ respectively. The domain of integration is $0 \leq x \leq 125, -20 \leq z \leq 20$.

disturbances, the problem has been solved numerically by a finite-difference method (for more details, see [15]). To identify the features of the quasi-periodicity of the pattern, we have chosen a long integration domain $H = 20$, $L = 125$ and applied the boundary conditions (8) which exclude the imposed periodicity of the resulting structure. The calculations were performed at uniform rectangular mesh 200 by 625. As the initial condition, we use a random field of the stream function with amplitude less than 10^{-3} .

The nonlinear evolution of the system can be best understood when studying the changes in the terms of the density given by (6). Figure 4 shows a consecutive restructuring of the density field over time. At the very beginning, the base state is absolutely stable, and the fluid convection is absent (Fig. 4, $t = 0.1$). However, two zones of low density are already clearly visible in the figure. The instability in the lower band is excited first. The pattern is a perfectly periodic system of chemoconvective cells enclosed between the layers of the motionless fluid (Fig. 4, $t = 0.5$). At this point in time, the wave number of the structure is about $k_1 \approx 2.46$, which agrees well with the linear stability analysis (see Fig. 3). Then, the instability #2 is excited in the upper density pocket. The wavenumber of this structure is much smaller: $k_2 \approx 0.5$ (Fig. 4, $t = 5$). When the latter instability develops sufficiently, it starts to affect the chemoconvection in the lower density pocket by injecting fresh acid with a spatial periodicity of $2\pi/k_2$. This leads to the formation of an obvious spatial quasi-periodic pattern below the reaction front (Fig. 4, $t = 5$ and 10). Finally, the pattern loses its regularity and is destroyed (Fig. 4, $t = 15$).

Let us define the coordinate x as a new effective time and consider the "dynamics" of the system. In addition to calculating the power spectrum, we perform the technique of the phase portrait reconstruction including the method of delays [21] with preprocessing using the singular value decomposition (SVD) method [22]. In this technique, a multi-dimensional embedding space is constructed from the time series data. The usage of the SVD method allows calculating an optimal basis for the projection of the reconstructed phase dynamics of the system. In our case, this analysis can be carried out only for a limited number of points (625) equal to the number of grid nodes along x . The signal for such an analysis was prepared as follows. The density field $\rho(t, x, z)$ has been spatially averaged across the lower instability band

$$\hat{\rho}(t, x) = \frac{1}{H_{bot}} \int_{-H_{bot}}^0 \rho(t, x, z) dz, \quad (16)$$

to yield the averaged profile $\hat{\rho}(t, x)$ depending on time t being the governing

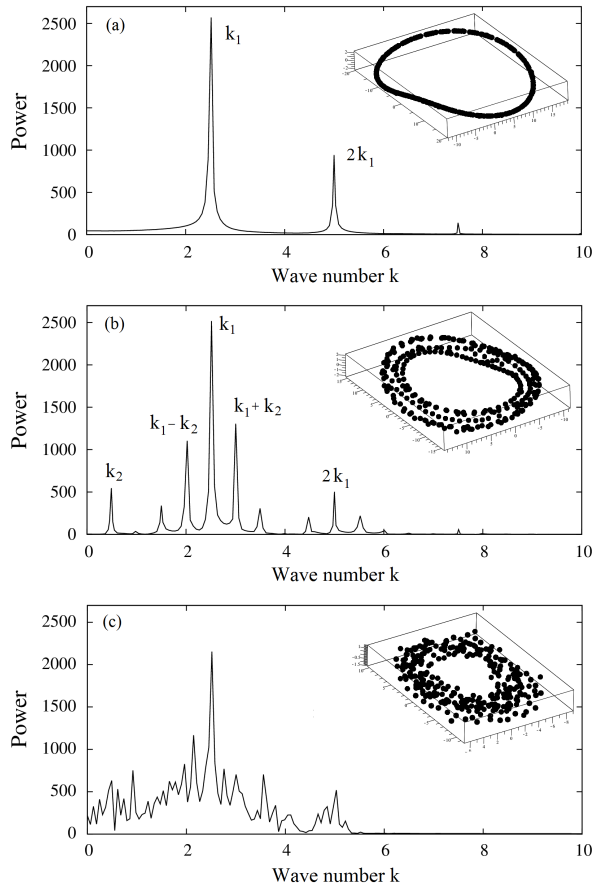


Figure 5: The power spectra and phase portraits (in *Inset*) reconstructed from the averaged density $\hat{\rho}(t, x)$ at three consecutive times: (a) $t = 0.5$; (b) $t = 5$; (c) $t = 15$.

parameter and the longitudinal coordinate x playing the role of effective time. Here, H_{bot} stands for the width of the lower instability zone.

Fig. 5 shows the Fourier spectra and phase portrait reconstructions calculated for three characteristic points in time. The dynamic mode in Fig. 5, $t = 0.5$ can be unambiguously characterized as periodic. The first peak of the power spectrum determines the authentic wave number of the 1st instability $k_1 \approx 2.46$, and the second one is simply the double value of the first peak. Thus, the transition from a stable base state (Fig. 4, $t = 0.1$) to a periodic system of chemoconvective cells (Fig. 4, $t = 0.5$) can be interpreted as a spatial Hopf bifurcation giving rise to a limit cycle shown in *Inset*. The following dynamic mode demonstrates obvious signs of a quasiperiodic behavior (Fig. 5, $t = 5$). The effect of the instability #2 is expressed in the fact that the power spectrum now contains two characteristic peaks and all other peaks are just their linear combinations. The peak in the long-wave part of the spectrum corresponds to the wave number $k_2 \approx 0.5$. Thus, the transition from the periodic cells (Fig. 4, $t = 0.5$) to a spatially quasi-periodic system of chemoconvective cells (Fig. 4, $t = 5$) can be interpreted as a secondary Hopf bifurcation giving rise to a two-dimensional torus shown in *Inset* of Fig. 5, $t = 5$. Since the “time series” based on $\hat{\rho}(t, x)$ is insufficient for studying the complex bifurcations that require long data sequences, we cannot assert whether another Hopf bifurcation to a three-dimensional torus is occurring reliably. But we can insist that the torus eventually collapses giving way to a toroidal strange attractor (Fig. 4, $t = 15$). Here the spectrum contains already continuous ranges of the excited waves characteristic of chaotic behavior.

Conclusions. – As it is well known, the Ruelle-Takens-Newhouse theory states that a typical transition to chaos involves two consecutive Hopf bifurcations resulting in a two-dimensional torus. As soon as the third Hopf bifurcation occurs, the broadband noise characteristic of a strange attractor should start to appear. However, this scenario is universal only for dynamic systems that evolve over time. In this paper, we demonstrate that exactly the same scenario can also be realized if the system evolves over space. This occurs in the physical system of two miscible solutions of HNO_3/NaOH , in which reaction-diffusion-convection processes lead to the appearance of spatially separated chemoconvective instabilities interacting with each other by means of diffusive signals. Since the instability wavelengths are independent parameters, the nonlinear interaction of the two modes leads to the appearance of a spatial quasiperiodic pattern, which is destroyed in accordance with

the Ruelle-Takens-Newhouse scenario.

We gratefully acknowledge the support of this work by the Russian Science Foundation Grant No. 19-11-00133.

References

- [1] K. Eckert, A. Grahn, Phys. Rev. Lett. **82**, 4436 (1999).
- [2] D.A. Bratsun, A. De Wit, Phys. Fluids **16**, 1082 (2004).
- [3] K. Eckert, M. Acker, Y. Shi., Phys. Fluids **16**, 385 (2004).
- [4] Y. Shi and K. Eckert, Chem. Eng. Sci. **63**, 3560 (2008).
- [5] D.A. Bratsun and A. De Wit, Chem. Eng. Sci. **66**, 5723 (2011).
- [6] L. Rongy, P. M. J. Trevelyan, and A. De Wit, Phys. Rev. Lett. **101**, 084503 (2008.)
- [7] A. Zalts, C. El Hasi, D. Rubio, A. Urena, and A. D’Onofrio, Phys. Rev. E **77**, 015304 (2008)
- [8] C. Almarcha, P.M.J. Trevelyan, P. Grosfils, and A. De Wit, Phys. Rev. Lett. **104**, 044501 (2010).
- [9] K. Tsuji and S. C. Müller, J. Phys. Chem. Lett. **3**, 977 (2012).
- [10] S. H. Hejazi, J. Azaiez, J. Fluid Mech. **695**, 439 (2012).
- [11] J. Carballido-Landeira, P. M. J. Trevelyan, C. Almarcha, and A. De Wit, Phys. Fluids **25**, 024107 (2013).
- [12] M. C. Kim, Chem. Eng. Sci. **112**, 56 (2014).
- [13] D. Bratsun, K. Kostarev, A. Mizev, and E. Mosheva, Phys. Rev. E, **92**, 011003 (2015).
- [14] P. M. J. Trevelyan, C. Almarcha, and A. De Wit, Phys. Rev. E, **91**, 023001 (2015).
- [15] D. A. Bratsun, O. S. Stepkina, K. G. Kostarev, A. I. Mizev, and E. A. Mosheva, Microgravity Sci. Technol. **28**, 575 (2016).

- [16] D. Bratsun, A. Mizev, E. Mosheva, and K. Kostarev, *Phys. Rev. E*, **96**, 053106 (2017).
- [17] D. Ruelle and F. Takens, *Commun. Math. Phys.*, **20**, 167 (1971).
- [18] S. Newhouse, D. Ruelle, and F. Takens, *Commun. Math. Phys.* **64**, 35 (1978).
- [19] J. Crank, *The Mathematics of Diffusion* (Clarendon, Oxford, UK, 1975).
- [20] C.T. Tan and G.M. Homsy, *Phys. Fluids* **29**, 2549 (1986).
- [21] N. H. Packard, J. P. Crutchfield, J. D. Farmer, and R. S. Shaw, *Phys. Rev. Lett.* **45**, 712 (1980).
- [22] D. S. Broomhead, G. P. King, *Physica D.* **20**, 217 (1986).